Journal of The Electrochemical Society, 158 (1) E1-E7 (2011)
0013-4651/2010/158(1)/E1/7/$28.00 © The Electrochemical Society

Direct Fabrication of High-Aspect Ratio Anodic Aluminum Oxide with Continuous Pores on Conductive Glass

Justin J. Hill,[a] Kelly Haller,[a] and Kirk J. Ziegler[a,b,*,z]

[a]Department of Chemical Engineering and [b]Center for Surface Science and Engineering, University of Florida, Gainesville, Florida 32611, USA

The role of metal interlayers in maintaining adhesion during the direct fabrication of anodic aluminum oxide (AAO) with *high*-aspect ratio pores on tin-doped indium oxide (ITO) is studied. Chromium and titanium interlayers can maintain adhesion while anodization is conducted in either sulfuric, oxalic, or phosphoric acid solutions. However, the ability to form high-aspect ratio pores is dependent on the interlayer and aluminum thickness, the method of aluminum deposition, and possibly the cleaning/surface treatment of ITO prior to aluminum deposition. AAO films approximately 2 μm thick were prepared in oxalic and phosphoric acids, yielding high-aspect ratio pores with length to diameter ratios of 47 and 14, respectively. The distinct stages of pore formation are also correlated with the time-resolved current response of the anodization cell, which provides in situ information about the anodization process so that adhesion can be maintained throughout pore formation. The direct fabrication of AAO on ITO/glass substrates from a single-step evaporation of *thick* aluminum films enables the formation of smooth and continuous gold nanowires, which have potential applications in photonics.
© 2010 The Electrochemical Society. [DOI: 10.1149/1.3506007] All rights reserved.

Manuscript submitted May 6, 2010; revised manuscript received October 5, 2010. Published November 9, 2010.

Fabrication of anodized aluminum is a common and widespread industrial practice. Anodic aluminum oxide (AAO) membranes, with cylindrical submicrometer pore diameters, are readily produced in the laboratory and are also commercially available.[1-6] Typically, AAO is fabricated from aluminum foil or sheets[7] and the excess aluminum after anodization can be dissolved, leaving a freestanding membrane.[1] The high pore density and surface area of AAO membranes are being used for a variety of research applications, including catalyst supports,[8] nanoscale filters, hierarchical molecular sieves,[9] and photonics.[10]

Competitive development of more powerful integrated circuits requires cost effective methods of increasing the device density.[11] The ordered structures, controllable pore diameters, and high density of pores in AAO membranes have led several researchers to use them for the fabrication of nanostructures.[12-22] While device fabrication using AAO is still in its infancy, this templated structure can provide a uniform and ordered architecture to facilitate the controlled growth of devices for applications, such as photovoltaic cells,[23] superconductivity, optical spectroscopy, and catalytic conversion of chemical to mechanical energy,[24] as well as core/shell nanostructures for ultrafast charge collection.[25] The incorporation of these structures onto a substrate is particularly important when considering AAO-templated nanostructure fabrication. Preparing arrays of nanostructures, such as nanowires, on varying substrates is a rapidly growing area of interest in fabricating functional, high-aspect and high surface-area devices. Whether electrical, mechanical, or optical functionality is required of the nanostructure array, both the nanostructure and substrate composition are defining parameters of device operation.

Early approaches in preparing vertical nanostructures through AAO templates were done by either directly mounting the membrane on the substrate[16,26] or blocking the pores on one side of the membrane prior to inclusion.[27,28] These approaches can give rise to device contamination from chemicals used to bond the AAO to the substrate and can lead to unwanted side reactions if electrochemistry is performed.[29] Furthermore, the planar interface between the bonded template and the support may not be conformal, leading to gaps between the substrate and the template. These gaps either prevent the fabrication of nanostructured devices on the support through the AAO template or hinder their performance.

Directly fabricating AAO onto a substrate eliminates the need to bond a freestanding template.[30-32] An important aspect unique to direct AAO/substrate formation is controlling the interface between the substrate and the anodized film. In addition to maintaining contact between the porous template and substrate, the pores must be completely anodized and the remaining aluminum oxide barrier layer must be removed if device contact characteristics are to be controlled or if freestanding nanostructure arrays are desired. The difficulty with fabricating AAO directly on a substrate, other than native aluminum, is the volume expansion of aluminum when oxidized during anodization. The volume of the film increases by 40%,[2] creating adhesion problems that can arise at any time during the anodization process. Delamination of either the Al or AAO from the substrate prevents the pores from forming or destroys the template because of localized electrochemical reactions.

Despite these problems, many researchers have directly fabricated AAO on Si supports without[33-38] and with differing inter- and sublayers.[39-45] Researchers have then used these AAO templated structures for the fabrication of nanowires.[33,40,45] A majority of the work has focused on the use of thin (⩽ 2 μm) Al films (see Ref. 46, for example). Xu and co-workers are one of the few researchers to use film thickness greater than 2 μm to construct AAO; however, they needed to construct an ultrahigh vacuum electron beam (E-beam) evaporation system.[38] The system was capable of Al film thicknesses of 50 μm, enabling the use of a two-step anodization procedure,[47] which enhances AAO pore ordering by sacrificing a portion of the Al layer. An interesting feature of anodizing Al on silicon supports is that the pore diameter is often less than what is obtained during anodization of Al foils. It has been postulated that this could be due to either differences in grain structure of the evaporated Al film[34] or strain propagation through the Al film due to lattice mismatch with the underlying substrate.[39,44,48]

While direct fabrication of AAO on Si substrates has been well established, many photonic applications require nanowire arrays on transparent conductive substrates. Unfortunately, adhesion problems during the anodization process are further exacerbated because tin-doped indium oxide (ITO) is not electrochemically inert to the anodizing solution.[30-32,49] The first example of direct fabrication of AAO on ITO was demonstrated by Chu et al.[49] They reported the successful fabrication of AAO in phosphoric acid from 2 μm thick aluminum films deposited by radio frequency (rf) sputtering, resulting in large diameter AAO pores.[30,49] A loose correlation between the time-resolved current response of Al/ITO anodization and aluminum foils was observed. One significant deviation they observed from the anodization of aluminum foil was that kinks and voids were observed in the AAO pores. This arose from the fact that the aluminum was deposited in two steps, creating an aluminum/aluminum film junction. In addition, the Al/ITO anodization suffered end-of-anodization sparking and gas evolution that frequently destroyed the film and increased the resistivity of the ITO.[49] Gas

* Electrochemical Society Active Member.
z E-mail: kziegler@che.ufl.edu

Downloaded 29 Dec 2010 to 159.226.100.225. Redistribution subject to ECS license or copyright; see http://www.ecsdl.org/terms_use.jsp

evolution and sparking could be mitigated by monitoring the time-resolved current response and ceasing anodization at the appropriate time. However, the current response between the complete anodization region and the initial stages of gas evolution and sparking is not well defined, making it difficult to control the process. Cho et al.[32] independently corroborated this work by following the same procedure.

Foong et al. recently enhanced the adhesion of AAO on ITO through the use of titanium interlayers during anodization of 200 nm aluminum films in either sulfuric, oxalic, or phosphoric acid solutions.[31] These three different anodizing solutions provide the ability to fabricate a wide range of pore diameters. Specifically, phosphoric acid typically produces pore diameters 100 nm and higher, while oxalic acid produces pore diameters between 25 and 75 nm and sulfuric acid produces pore diameters on the order of 10 nm.[2]

The ability to directly fabricate AAO pores on ITO with varying pore depth and diameter is a crucial step toward the fabrication of nanostructures with a wide variety of tunable aspect ratios for photonic applications where a transparent and conductive substrate is required. Foong et al. have demonstrated that the use of titanium adhesion layers prevents delamination during anodization for *thin* aluminum films on ITO.[31] However, the aim of this study is to fabricate *thick* AAO films directly on a transparent conductive support with deep pores and adjustable pore diameter. This is an important step toward fabricating nanostructures with tunable aspect ratios. It is shown in this study that both interlayers of Ti and Cr can be used as adhesion layers during the anodization of aluminum on ITO. However, only certain combinations of anodization solution, interlayer thickness and composition, and aluminum thickness are found to successfully fabricate AAO on ITO/glass substrates. In addition, we find that seemingly minor deviations during film deposition can change the anodization process.

Experimental

Deposition of aluminum and interlayers.— Porous AAO films were fabricated on transparent conductive substrates via the electrochemical oxidation of evaporated or rf-sputtered aluminum films. The transparent conductive substrate was composed of ITO on 0.11 cm thick glass substrates, which were obtained precut (Thin Film Devices, Inc.) with dimensions of 1.25×5 cm, an ITO film thickness of 450 ± 15 nm, and a sheet resistance $<5\ \Omega/\text{cm}^2$. Prior to metal deposition, the substrates were carefully degreased by sonication for 20 min each in soapy deionized water, acetone, ethanol, and then deionized water. The substrates were then placed in either a Kurt J. Lesker CMS-18 sputter deposition or a custom E-beam evaporation chamber capable of moderate vacuum pressures. For sputtered films, the substrates were vacuumed to 2×10^{-8} Torr and aluminum was deposited at 1.8 Å/s to the desired thickness. E-beam evaporation was carried out at 5×10^{-6} Torr. Chromium or titanium interlayers were deposited at 0.5 ± 2 Å/s [monitored and shut-off controlled by a quartz crystal microbalance (QCM)] to a thickness of 0.3, 1, or 10 nm. Based on the time to close the QCM-controlled shutter, it is estimated that the error in final thickness is one-tenth of the deposition rate. Immediately following interlayer deposition and without breaking chamber vacuum, 99.999% pure aluminum was evaporated at a rate of 10 or 200–300 nm/s to a thickness of either 0.2 or 2.2 μm, respectively. In some cases, the E-beam evaporated films were thermally oxidized in a muffle furnace (Barnstead) at 450°C for 30 min to form a thick oxide layer on the surface prior to anodization.

In all the cases, a portion of the substrate was then covered with an aluminum foil to expose a 1×1.25 cm strip, where a 10 μm layer of silica was evaporated at a rate of 100–200 nm/s. This silica strip is used to provide electrical insulation to prevent anodization of the aluminum film at the interface between air and the anodizing solution. Otherwise, electrochemical oxidation of the films occurs too rapidly at this interface and electrical contact with the submerged portion of the film is cut off due to the destruction of the ITO on the glass substrate at the air–solution interface.[50]

Anodization and pore widening.— Following film deposition, the substrates were placed in either 1.3 M phosphoric acid (7°C), 0.3 M oxalic acid (2°C), or 0.2 M sulfuric acid (2°C) solutions held at temperature in a jacketed beaker by a recirculating chiller. The solution was stirred at a rate of 450 rpm. The substrate was inserted, so the fluid flow impinged normal to the aluminum film and the silica strip bridged the air–solution interface. A carbon counter-electrode was used for all anodization processes. Aluminum films with interlayers were anodized at a constant voltage of 35, 60, or 130 V using a Lambda Gen 300-5 power supply for sulfuric, oxalic, and phosphoric acid solutions, respectively. Aluminum films anodized without interlayers were anodized at a constant voltage of 80 V in phosphoric acid. The potential was increased at a rate of 4 V/s to the final voltage, and the current was monitored with a Laurels amp-meter and a custom-made LABVIEW control program. Upon complete anodization of the AAO on ITO substrates, the alumina barrier layer was etched with 5 wt % phosphoric acid for 330 s to open the bottom of the pore.

Electrochemical nanowire synthesis.— Gold nanowires were synthesized by electrochemically depositing gold from solution (Technigold 25 ES, Technic Inc.) onto the exposed ITO layer within the pores of the AAO template. The solution was held at 60°C and deposition was performed potentiostatically (Versastat V3, Princeton Applied Research) against a carbon counter-electrode at −0.5 V versus a saturated calomel electrode. The deposition current was monitored closely so that gold deposition was ceased once the current began to rise dramatically, resulting in completely filled AAO template pores.[51] In some cases, the template was removed using a newly developed method that prevents aggregation of the nanowires.[52]

Characterization.— Field emission scanning electron microscopy (FESEM) micrographs were obtained on a JEOL JSM 6400. Aluminum films that appeared to have undergone oxidation during deposition, especially sputtered aluminum, were analyzed by FESEM as well as XPS (Perkin-Elmer PHI 5100 ESCA system) to quantify the degree and type of oxidation. Sheet resistance was measured with a Princeton Applied Research VersaSTAT 3 potentiostat and tungsten probes. Light transmittance was collected with a Perkin-Elmer Lambda 9 UV/Vis/NIR spectrophotometer.

Results

Various film thicknesses and anodization conditions are used to fabricate high-aspect AAO pores on ITO. Table I summarizes the anodization results for each combination of anodization solution, interlayer material and thickness, as well as the final AAO film layer thickness. Details of the results are discussed further below. Each condition presented in Table I was repeated a minimum of six times to ensure the accuracy of the results. Although not all diameter/length combinations were successful, aspect ratios of approximately 1.4, 8.3, 14, 18, and 47 were obtained. These aspect ratios of AAO on ITO expand those obtained by Foong et al.,[31] accomplishing the primary goal of high-aspect ratio pores.

Prepore formation and postpore formation failures listed in Table I refer to the point during the process at which anodization failed. Prepore formation failure generally occurred due to either a higher selectivity of the interlayer to electrochemical reaction than the aluminum film or immediate electrical discharge across the film. Postpore formation failure occurred because the interlayer dissolved, removing the anodized layer from the substrate, or because arcing and gas evolution locally destroyed the film, leaving only a small fraction of the AAO film intact. A more detailed description of these failures is outlined in the supplementary information.[50]

Direct fabrication of AAO on ITO without interlayers.— Aluminum was rf-sputtered in a single deposition step to thicknesses

Downloaded 29 Dec 2010 to 159.226.100.225. Redistribution subject to ECS license or copyright; see http://www.ecsdl.org/terms_use.jsp

Table I. Anodization results in various acids for aluminum films of varying thickness on ITO using either titanium or chromium interlayers. Note: the aspect ratio (L/D) for successful anodizations are reported based on the actual AAO film thickness, not the initial aluminum film thickness.

Interlayer	Aluminum film thickness (μm)	Sulfuric acid	Oxalic acid	Phosphoric acid
no interlayer[a]	1	—	—	D = 55 nm; L/D = 18
	2.2	—	—	Failure[b]
10 nm Ti	0.2	D = 21 nm; L/D = 8.3	Failure[c]	Failure[d]
	2.2	Failure[d]	D = 45 nm; L/D = 47	Failure[d]
10 nm Cr	0.2	Failure[c]	Failure[d]	D = 145 nm; L/D = 1.4
	2.2	Failure[c]	Failure[d]	D = 145 nm; L/D = 14

[a] RF-sputter deposition (anodized at 80 V in phosphoric acid).
[b] No pore formation.
[c] Postpore formation failure.
[d] Prepore formation failure.

greater than 1 μm on bare ITO. Single-step deposition was used to avoid the kinks and voids observed previously at the interfaces of multilayer Al films.[49] The rf-sputtered aluminum was then anodized in phosphoric acid at 80 V. Anodization occurred without failure for sputtered aluminum films thinner than 1.1 μm, although a small amount of delamination is observed at the side of the substrate. Above this thickness, the anodization resulted in the continuous oxidation and dissolution of the aluminum oxide. These films never appeared to form pores based on the time-resolved current response, and there was no film left on the substrate after the anodization was complete. E-beam evaporation was also used to prepare aluminum films directly on ITO. However, anodization of E-beam evaporated aluminum films of any thickness resulted in significant delamination of the film.

Direct fabrication of AAO on ITO using interlayers.— Given the limited success of the direct fabrication of AAO on ITO, interlayers were used in an approach similar to that of Foong et al.[31] The authors used Ti interlayers to fabricate thin (0.2 μm) AAO on ITO, observing the best results when the Ti interlayer thickness was 0.3 nm. However, our attempts to anodize films with Ti interlayer thicknesses of either 0.3 or 1 nm were unreliable. Therefore, a thicker titanium interlayer of 10 nm was used during all anodization experiments described below. The FESEM image in Fig. 1a confirms that anodization of 0.2 μm Al on Ti/ITO is successful at maintaining adhesion during anodization in sulfuric acid. As seen in the titanium interlayer where AAO was scratched away, anodization also reacts with the titanium layer, resulting in dimples that expose the underlying ITO. The size of the dimples is approximately 20 nm, matching the pore diameter of the AAO pore. On the other hand, the anodization of 0.2 μm Al on Ti/ITO in oxalic and phosphoric acids failed, contrary to the prior work of Foong et al.[31]

Interestingly, different anodization results are obtained when thicker Al films of 2.2 μm are used with Ti interlayers. As shown in Table I, anodization fails again in phosphoric acid; however, both oxalic and sulfuric acids have reversed outcomes when compared to thinner Al films. These thicker Al layers now result in failure for sulfuric acid while anodization in oxalic acid is now successful. The FESEM image in Fig. 1b is a side-view image of the AAO film obtained for the anodization of 2.2 μm Al on Ti/ITO in oxalic acid. This image clearly shows the high degree of adhesion between the AAO and the substrate, yielding a dense array of ~45 nm diameter pores directly fabricated on the ITO substrate. Interestingly, this pore diameter is much lower than expected for the same anodization conditions conducted with only an aluminum foil. This phenomenon has been observed in the anodization of Al on Si substrates. These differences in pore size have been attributed to grain structure[34] or the propagation of lattice mismatch strain.[39,44,48] Lattice strain propagation seems likely in our experiments since delamination occurred prior to pore formation when anodizing Al directly on ITO.

In a further attempt to broaden the range of pore diameters and lengths obtained for AAO films on ITO, anodization experiments were also conducted for 10 nm Cr interlayers in each acid solution. As shown in Table I, the anodization was successful in phosphoric acid for both 0.2 and 2.2 μm aluminum films. The FESEM images in Fig. 1c show the 2.2 μm aluminum films anodized in phosphoric acid. The barrier layer for these AAO films is on the same order of thickness as the diameter of the pore. The side-view image shows that this anodization also maintained a high degree of adherence to the Cr/ITO substrate, yielding a directly fabricated AAO film with a dense array of ~145 nm diameter pores. Again, the pore diameter is smaller than expected for the equivalent anodization of aluminum films.

The image of the AAO/interlayer/ITO substrate in Fig. 1d shows that thick AAO films on ITO maintain high transmittance and that adhesion is uniform over the entire substrate with few defects. The optical transmittance (%T) spectra for films anodized in different acid solutions are shown in Fig. 1e. The spectra show oscillations that have a specific frequency, which are due to interference patterns from the ordered AAO structure.[53] AAO films anodized in sulfuric, oxalic, and phosphoric acids have approximate transmittance values of 75%, 70%, and 65% at 900 nm, respectively. As expected, thinner AAO films (sulfuric acid, curve 1) have higher transmittance than the thicker AAO films. The transmittance for the thin AAO remains relatively constant at all wavelengths; however, the transmittance for thicker AAO films tends to decrease in transmittance at lower wavelengths. The anodization conditions also control the pore diameter (see Table I). Therefore, these decreases could be due to photon scattering from the AAO, which would be dependent on the pore diameter and periodicity. Indeed, larger pore diameters show more significant decreases in transmittance at lower wavelengths.

After barrier layer removal and pore widening, the tops of the pores are observed more clearly. As shown in the top-down SEM image in Fig. 1f, the pores in these thicker AAO films have high density. The pores do not exhibit uniform diameters or spacing; however, this may possibly be improved with surface modification prior to anodization[3,4,47] or two-step anodization.[47]

Successfully anodized substrates were placed in 25 wt % phosphoric acid for 2 h to completely remove the AAO template and evaluate the sheet resistance of the ITO substrate to determine if the anodization process altered the transparent conductive layer. The initial ITO on glass had a sheet resistance of 5 Ω/cm^2. Regardless of the conditions of anodization, there was only a small increase in substrate sheet resistance to ~9 Ω/cm^2. This minor increase in resistance should not significantly effect the electrodeposition of materials into the pores.

Downloaded 29 Dec 2010 to 159.226.100.225. Redistribution subject to ECS license or copyright; see http://www.ecsdl.org/terms_use.jsp

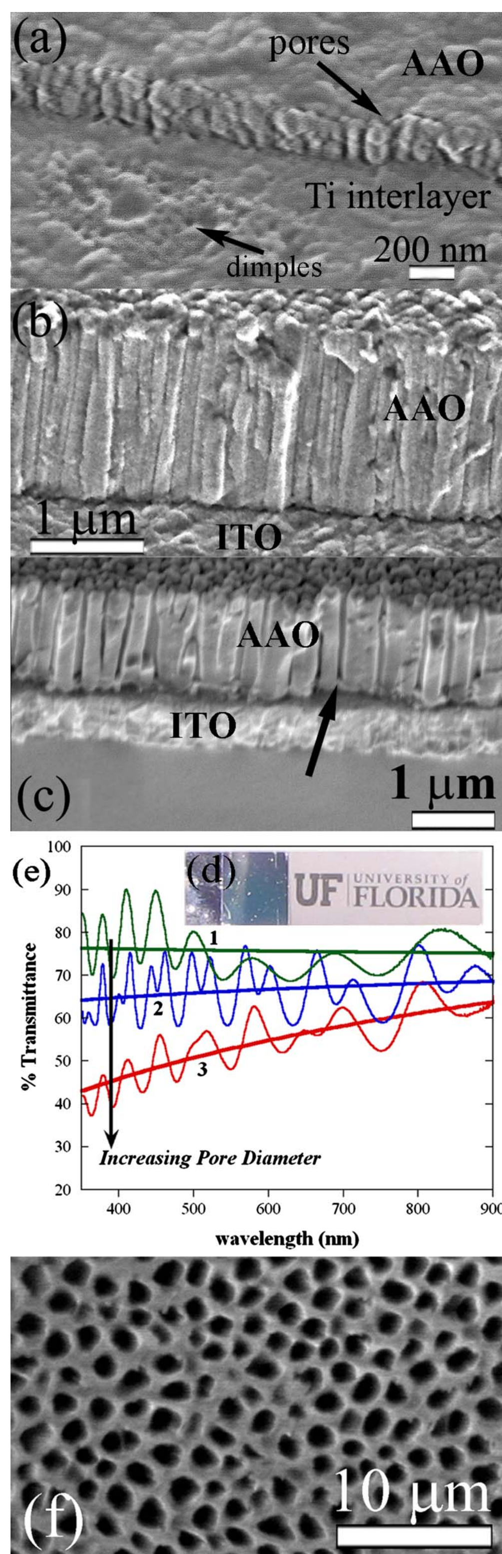

Figure 1. (Color online) Side-view FESEM images of (a) 0.2 µm Al/10 nm Ti/ITO anodized in sulfuric acid, (b) 2.2 µm Al/10 nm Ti/ITO anodized in oxalic acid, and (c) 2.2 µm Al/10 nm Cr/ITO anodized in phosphoric acid. The arrow pointing to the barrier layer shows that the barrier layer thickness is on the same order as the respective pore diameter. (d) The optical image shows that adhesion is maintained over the entire substrate. The transmittance of each film (e) shows that the substrates retain a high degree of transparency for films 1, 2, and 3 corresponding to the FESEM images in (a), (b), and (c), respectively. (f) FESEM image after pore widening shows that the AAO film has a high density of pores.

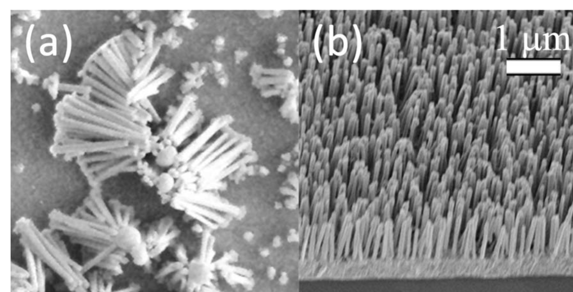

Figure 2. FESEM images of gold nanowires fabricated within the pores of AAO on ITO (a) after dissolving the template and (b) after using electric fields to prevent aggregation of the nanowires. The template was prepared by anodization of 2.2 µm Al on 10 nm Cr/ITO/glass substrates in phosphoric acid. Note that the nanowires are smooth and continuous.

Nanowire arrays are readily fabricated within the AAO on these conductive substrates. To demonstrate this, gold was electrochemically deposited into the AAO/ITO/glass substrate to form a gold nanowire array. Figure 2 shows FESEM images of the gold nanowire arrays obtained from the templates after dissolving the template (see Fig. 2a) or applying a simple method to prevent nanowire array aggregation during template removal (see Fig. 2b).[52] As can be seen in Fig. 2a, the gold nanowires are smooth and continuous along their length.

Discussion

Time-resolved current response during anodization of aluminum on ITO.— The time-resolved current response of the electrochemical cell provides detailed information concerning the processes that are occurring within the aluminum film during anodization. Once the changes in the current output are correlated to the processes occurring during anodization, time-resolved current data can serve as an active "litmus test" indicating whether the anodization is proceeding successfully.

Although the mechanism of AAO pore formation on substrates was previously outlined by Chu et al.,[49] it is more clearly depicted in the time-resolved current response when interlayers are used to maintain adhesion to the ITO substrate, as shown in Fig. 3. The shape of the current output shows four distinct processes occurring during the anodization of the aluminum film on ITO. The first three processes are similar to those observed for anodization of Al foils. The initial drop in current density is due to a negative current drift associated with the linear voltage ramp to the set-point voltage and is not one of these processes. In stage I, a planar surface oxide forms on the aluminum film. The resistance of the electrode increases as the surface oxide layer continues to grow, causing a dramatic decrease in the current density. This surface oxide layer can prevent further electrochemical oxidation of the aluminum; however, a large interfacial electric field forces the surface morphology to change from a planar film to a dimpled array, which is the onset of stage II.[6] This change in surface morphology allows the surface oxide thickness at the bottom of the pores to remain relatively constant, so the diffusion of aluminum and oxygen through the oxide layer can still be driven by the electric field, allowing the electrochemical oxidation of aluminum to continue.

Once the dimples form in the surface layer, the electrochemical reaction preferentially occurs at these sites. As these dimples continue to bore into the aluminum and grow into a fully formed pore (stage II), the active surface area increases substantially. This increase in electrode surface area gives rise to the increase in current density shown in Fig. 3 since the current density is relative to the initial planar electrode surface area. Shortly after pore initiation, the continued growth of the pores does not cause any increase in active electrode surface area (stage III). During this stage, the pores bore toward the substrate and the current remains constant because there

Downloaded 29 Dec 2010 to 159.226.100.225. Redistribution subject to ECS license or copyright; see http://www.ecsdl.org/terms_use.jsp

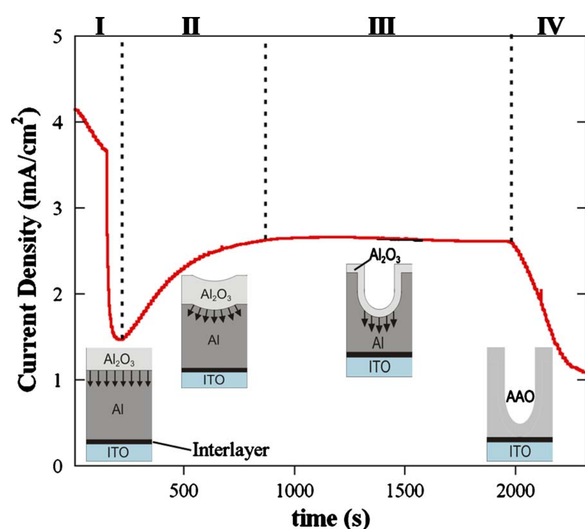

Figure 3. (Color online) A typical chronoamperometric response of a thick aluminum/interlayer film on ITO (shown here for 2.2 μm Al/10 nm Cr/ITO in phosphoric acid). This response depicts the overall mechanism that occurs during anodization: (I) current drop due to oxide growth and increasing substrate resistance to charge transfer; (II) pore initiation resulting in a dramatic increase in film surface area; (III) uniform pore growth; and (IV) current decrease due to increased resistivity from depletion of Al between the substrate and electrolyte. Note that drawings are not to scale.

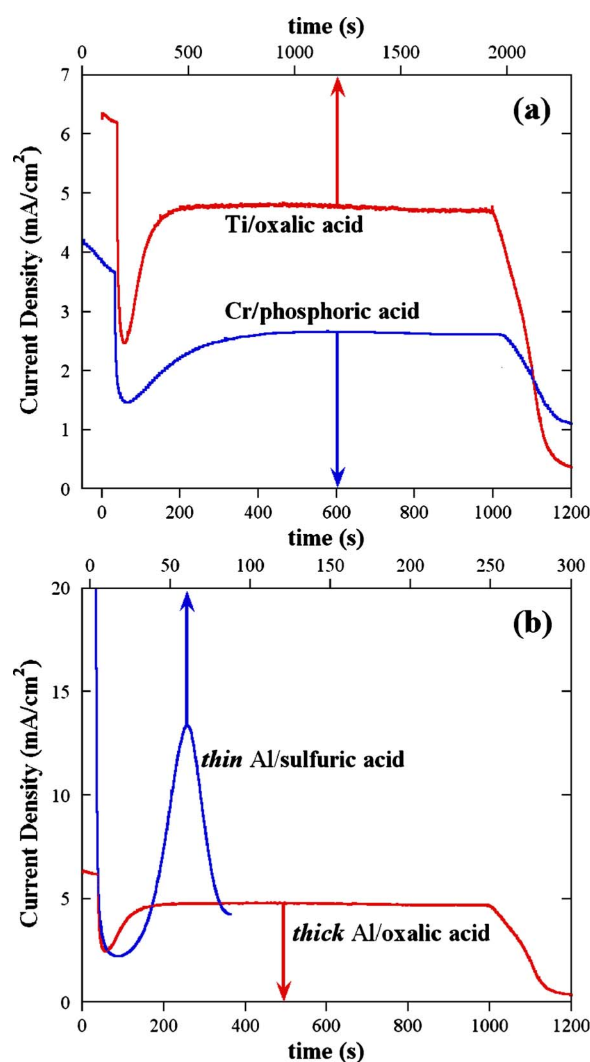

Figure 4. (Color online) The chronoamperometric response for anodization of (a) 2.2 μm Al on either 10 nm Cr or Ti interlayers in phosphoric or oxalic acid, respectively. The general trend is independent of interlayer composition and anodization conditions, indicating that the response is primarily due to internal aluminum film/pore growth processes. (b) 0.2 μm and 2.2 μm Al on 10 nm Ti interlayers anodized in sulfuric or oxalic acid, respectively. These results show how stages (II) and (IV), depicted in Fig. 2, can overlap and cancel one another out to obtain results similar to Foong et al.[31]

is no change to electrode surface area. This constant current is similar to the pore growth stage in Al foils, which was not observed by Chu et al.[49] because of the use of multilayer Al deposition. Finally, as anodization nears completion (stage IV), the current falls off rapidly. This drop is due to the diminishing amount of aluminum remaining in the film as it is thinned, which increases the sheet resistance. The remaining aluminum is oxidized, leaving behind a barrier layer. At this point, film arcing and gas evolution can occur, as observed by Chu et al.[49] In the absence of an interlayer, this arcing can be observed in stage III, causing severe damage to the overall film by the end of stage IV. However, the presence of an interlayer delays the arcing and gas evolution until the end of stage IV or beyond. Thus, this detrimental behavior is more easily averted by monitoring the current output and stopping the process before the current begins to increase at the end of stage IV.

When successful anodization occurs, the characteristic features depicted in Fig. 3 are independent of the anodization acid solution, applied voltage, interlayer material, and aluminum film thickness. These time-resolved current features are observed in all successful anodization scenarios because it involves processes occurring within the aluminum oxide/aluminum film. Deviations to the anodization acid solution, applied voltage, and aluminum film thickness only alter the overall anodization time and magnitude of the current density. For example, Fig. 4a depicts the time-resolved current response of the successful anodization of 2.2 μm aluminum films in oxalic and phosphoric acids with titanium and chromium interlayers, respectively. These time-resolved current responses are qualitatively equivalent, indicating that the overall mechanism for AAO formation on ITO in the presence of an interlayer is independent of the interlayer composition, anodization voltage, and acid solution.

While the qualitative features of the time-resolved current response are similar, the rate of current changes is likely indicative of the uniformity in pore initiation and growth across the entire substrate. The changes in current density in Fig. 4a associated with stage II surface reconstruction and stage IV barrier layer formation (see Fig. 3) have different slopes for different anodization conditions. The AAO formed in oxalic acid has sharp transitions between each stage, while the AAO formed in phosphoric acid shows gradual transitions between each stage in the pore formation process. The fast rate of pore formation (large positive slope in stage II) in oxalic acid indicates that all pores form at approximately the same time and at the same rate. Since all the pores start at the same time and grow at the same rate, the anodization process also reaches the substrate at the same time, resulting in a sharp decrease in current density. The gradual transitions associated with anodization in phosphoric acid indicate that not all pores are reaching the substrate at the same time. These differences could be important in maintaining adhesion since film arcing and delamination can start to occur once the anodization process reaches the substrate locally.

The primary differences in the time-resolved current responses observed in Fig. 3 and 4a from prior work[30,31,49] are in the pore initiation and uniform pore growth stage. Chu et al.[49] observed two peaks in current at the midpoint of stage III in aluminum films without an interlayer. These features are likely related to the lateral defects in the pores caused by the two-step Al deposition. In this study, a continual increase in current is observed shortly after the anodization process begins when thicker aluminum films are rf-sputtered in a single step without an interlayer. This continual in-

Downloaded 29 Dec 2010 to 159.226.100.225. Redistribution subject to ECS license or copyright; see http://www.ecsdl.org/terms_use.jsp

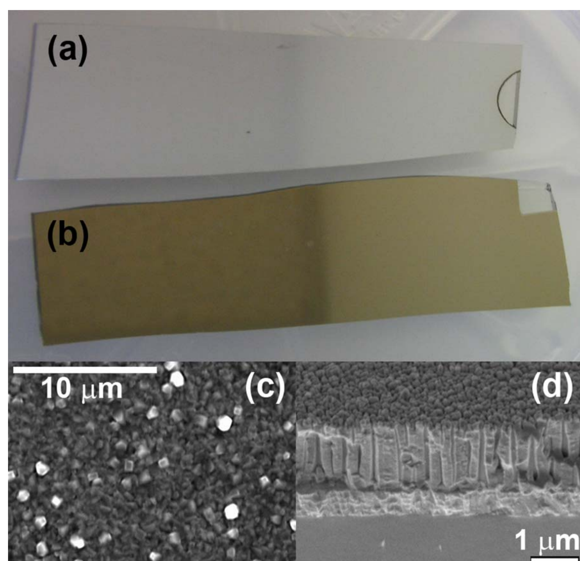

Figure 5. (Color online) Sputtered aluminum films deposited continuously up to thicknesses of (a) 5 μm and (b) 0.5 μm. The 5 μm film shows that a significant amount of oxidation has occurred as a result of the sputter deposition, which is not present with the thinner 0.5 μm film. FESEM imaging (c) shows at film thicknesses greater than 1.1 μm that aluminum oxide grains are dispersed throughout the film, which hinders anodization. However, the side-view FESEM image in (d) shows that surface oxidation (30 min, 450°C) of E-beam deposited Al films can be successfully anodized.

crease in current is likely the cause or the result of film delamination, exposing both sides of the deposited aluminum film as well as additional current from continual film delamination.

Foong et al.[31] did not observe a clear time-resolved current response associated with pore initiation and growth (stages II and III) likely because the aluminum films being anodized were only 0.2 μm thick. Thus, the increase in current from pore initiation and decrease in current due to barrier layer formation essentially cancel one another, keeping the current from rising. Figure 4b depicts this behavior when the time-resolved current responses of the 0.2 and 2.2 μm films are compared. As can be seen for the 0.2 μm in Fig. 4b, stages II and IV overlap and the galvanostatic region that is observed for the thicker film is not present.

Avoiding failure during anodization.— It was observed in this study that minor deviations create difficulties in repeating some of the prior work in the field, which highlights the importance of ITO surface treatment in the direct fabrication of AAO. As described below, different deposition methods (sputtering versus E-beam), aluminum thickness, or surface treatments prior to Al film deposition give different results.

While sputtered aluminum films may provide enhanced adhesion due to the high energy impact of the film deposition process,[31] the low deposition rate gives rise to significant substrate heating that may cause oxide formation when depositing more than 1.1 μm of aluminum. Although not explicitly stated, this may be the reason that prior aluminum films prepared on ITO by sputtering were deposited in 1 μm steps.[13,30,32,49] Indeed, the 5 μm Al film shown in Fig. 5a is white, indicating that a high degree of oxidation has occurred during the sputter deposition process. On the other hand, the 500 nm Al film shown in Fig. 5b is highly reflective, indicating that very little aluminum oxide is present. Several different thicknesses of aluminum were sputtered, which showed that film thicknesses greater than 1.1 μm no longer appear pristine or reflective. This is supported by the FESEM image in Fig. 5c of a sputtered, 1.1 μm aluminum film showing grains of aluminum, aluminum oxide, and possibly mixed aluminum/aluminum oxide. The presence of aluminum and aluminum oxide in the film was also confirmed with XPS.

Anodization of sputtered aluminum films thicker than 1.1 μm began to show delamination problems. At thicknesses greater than 1.5 μm, anodization was unsuccessful. Given that aluminum oxide began to form when film thickness exceeded 1.1 μm, it is believed that anodization failure for sputtered films is a result of random mechanical stresses imposed by the aluminum oxide grains dispersed within the bulk of the film (see Fig. 5c). To support this conclusion, pristine E-beam evaporated 2.2 μm Al on Cr films were thermally oxidized to produce a thick aluminum oxide film on the surface before anodization. These substrates appeared white from aluminum oxide and were similar in appearance to those in Fig. 5a. However, Fig. 5d shows that these substrates were successfully anodized in phosphoric acid, following the thermal growth of a thick surface aluminum oxide. Thus, thick surface oxides do not prevent AAO formation, indicating that the anodization failure observed for sputtered aluminum films is due to aluminum oxide grains dispersed within the bulk film.

While the requirement of film homogeneity could have been anticipated, the sensitivity of anodization to the thickness of the Al film was unexpected. These changes to anodization with thickness may be due to changes in the additional electrochemical resistance (i.e., potential drop) along the length of the pore. This electrochemical resistance increases with either decreasing pore diameter or increasing pore length. Anodization in sulfuric acid yields very small pores, resulting in large potential drops. The large potential drop could possibly slow down the electrochemical diffusion/reaction, resulting in charge buildup. This effect would not be problematic for Al foils but could lead to electrical discharge (prepore formation failure) when interlayers are used. Similarly, changes in electrochemical resistance may also explain the different behavior observed during anodization in oxalic acid. In this case, larger pores are formed in oxalic acid than in sulfuric acid. At the same Al thickness, oxalic acid would have less resistance. Therefore, at the end of pore formation, there is a greater driving force for electrochemical diffusion/reaction in oxalic acid. This increased driving force can cause arcing and gas evolution (postpore formation failure). Increasing the thickness of the aluminum reduces the driving force at the end of pore formation, minimizing the damage from these effects. These results suggest that there may be thickness regimes for successful anodization or that the electrochemical reactions need to be carefully controlled.

Finally, the inability to reproduce all of the work of Foong et al. for 0.2 μm Al films may be due to the difference in ITO degreasing and surface treatments.[31] The degreasing procedure used here was benign in comparison to the plasma surface treatment used by Foong et al. This high energy cleaning method may be the reason why they could maintain adhesion with titanium interlayers in all three anodization acid solutions.

Conclusion

This study demonstrates the dependence of interlayer composition and the thickness of the aluminum layer on the adhesion of AAO directly fabricated on ITO/glass substrates. Chromium interlayers provide excellent adhesion during anodization in phosphoric acid solutions but fail in oxalic and sulfuric acids. On the other hand, titanium interlayers fail during anodization in phosphoric acid and succeed in either oxalic or phosphoric acids. However, these anodization processes are dependent on not only the acid solution but also the thickness of the aluminum. For example, anodization of 0.2 μm Al films in oxalic acid fails while thicker Al films are successful. Despite these difficulties, longer pores have been formed on ITO without delamination of AAO. The highest aspect ratio of pores was obtained when anodized in oxalic acid. The differences between this study and prior work could also highlight the importance of surface treatment/cleaning in this process. The adhesion of AAO on ITO appears to be extremely sensitive to the surface treatment of the ITO, regardless of the adhesion layer used.

Downloaded 29 Dec 2010 to 159.226.100.225. Redistribution subject to ECS license or copyright; see http://www.ecsdl.org/terms_use.jsp

Acknowledgments

We acknowledge funding from the University of Florida Opportunity Fund and the Donors of the American Chemical Society Petroleum Research Fund (ACS-PRF).

University of Florida assisted in meeting the publication costs of this article.

References

1. O. Jessensky, F. Muller, and U. Gosele, *Appl. Phys. Lett.*, **72**, 1173 (1998).
2. A. P. Li, F. Muller, A. Birner, K. Nielsch, and U. Gosele, *J. Appl. Phys.*, **84**, 6023 (1998).
3. H. Masuda, H. Asoh, M. Watanabe, K. Nishio, M. Nakao, and T. Tamamura, *Adv. Mater.*, **13**, 189 (2001).
4. H. Masuda, H. Yamada, M. Satoh, H. Asoh, M. Nakao, and T. Tamamura, *Appl. Phys. Lett.*, **71**, 2770 (1997).
5. Jp Osulliva and G. C. Wood, *Proc. R. Soc. London, Ser. A*, **317**, 511 (1970).
6. V. P. Parkhutik and V. I. Shershulsky, *J. Phys. D*, **25**, 1258 (1992).
7. H. B. Xu, H. Z. Chen, W. J. Xu, and M. Wang, *Chem. Phys. Lett.*, **412**, 294 (2005).
8. P. Stair, C. Marshall, G. Xiong, H. Feng, M. Pellin, J. Elam, L. Curtiss, L. Iton, H. Kung, M. Kung, et al., *Top. Catal.*, **39**, 181 (2006).
9. S. A. Bagshaw, E. Prouzet, and T. J. Pinnavaia, *Science*, **269**, 1242 (1995).
10. L. K. Teh, V. Furin, A. Martucci, M. Guglielmi, C. C. Wong, and F. Romanato, *Thin Solid Films*, **515**, 5787 (2007).
11. G. E. Moore, *Electronics*, **38**, 114 (1965).
12. J. J. Hill, S. P. Cotton, and K. J. Ziegler, *Chem. Mater.*, **21**, 1841 (2009).
13. S. Z. Chu, S. Inoue, K. Wada, D. Li, H. Haneda, and S. Awatsu, *J. Phys. Chem. B*, **107**, 6586 (2003).
14. G. Z. Cao, *J. Phys. Chem. B*, **108**, 19921 (2004).
15. Y. Ishikawa and Y. Matsumoto, *Sol. Stat. Ion.*, **151**, 213 (2002).
16. Y. Liang, C. Zhen, D. Zou, and D. Xu, *J. Am. Chem. Soc.*, **126**, 16338 (2004).
17. S. J. Limmer, T. P. Chou, and G. Z. Cao, *J. Mater. Sci.*, **39**, 895 (2004).
18. S. J. Limmer, S. Seraji, Y. Wu, T. P. Chou, C. Nguyen, and G. Z. Cao, *Adv. Funct. Mater.*, **12**, 59 (2002).
19. Y. L. Qingmin Zhang, Xu. Dongsheng, and Gu. Zhennan, *J. Mater. Sci. Lett.*, **20**, 925 (2001).
20. G. Xomeritakis, N. G. Liu, Z. Chen, Y. B. Jiang, R. Kohn, P. E. Johnson, C. Y. Tsai, P. B. Shah, S. Khalil, S. Singh, et al., *J. Membr. Sci.*, **287**, 157 (2007).
21. K. J. Ziegler, B. Polyakov, J. S. Kulkarni, T. A. Crowley, K. M. Ryan, M. A. Morris, D. Erts, and J. D. Holmes, *J. Mater. Chem.*, **14**, 585 (2004).
22. Y. Wu, G. Cheng, K. Katsov, S. W. Sides, J. Y. Wang, J. Tang, G. H. Fredrickson, M. Moskovits, and G. D. Stucky, *Nature Mater.*, **3**, 816 (2004).
23. A. B. F. Martinson, J. W. Elam, J. T. Hupp, and M. J. Pellin, *Nano Lett.*, **7**, 2183 (2007).
24. T. R. Kline, M. Tian, J. Wang, A. Sen, M. W. H. Chan, and T. E. Mallouk, *Inorg. Chem.*, **45**, 7555 (2006).
25. M. Lahav, E. A. Weiss, Q. Xu, and G. M. Whitesides, *Nano Lett.*, **6**, 2166 (2006).
26. Z. Miao, D. S. Xu, J. H. Ouyang, G. L. Guo, X. S. Zhao, and Y. Q. Tang, *Nano Lett.*, **2**, 717 (2002).
27. Y. Yang, H. Chen, Y. Mei, J. Chen, X. Wu, and X. Bao, *Solid State Commun.*, **123**, 279 (2002).
28. M. J. Zheng, L. D. Zhang, G. H. Li, X. Y. Zhang, and X. F. Wang, *Appl. Phys. Lett.*, **79**, 839 (2001).
29. U. Evans, P. E. Colavita, M. S. Doescher, M. Schiza, and M. L. Myrick, *Nano Lett.*, **2**, 641 (2002).
30. S. Z. Chu, K. Wada, S. Inoue, and S. Todoroki, *Electrochim. Acta*, **48**, 3147 (2003).
31. T. R. B. Foong, A. Sellinger, and X. Hu, *ACS Nano*, **2**, 2250 (2008).
32. S. I. Cho, R. Xiao, and S. B. Lee, *Nanotechnology*, **18**, 405705 (2007).
33. T. Shimizu, Z. Zhang, S. Shingubara, S. Senz, and U. GoÌsele, *Nano Lett.*, **9**, 1523 (2009).
34. A. F. Feil, M. V. da Costa, L. Amaral, S. R. Teixeira, P. Migowski, J. Dupont, G. Machado, and S. B. Peripolli, *J. Appl. Phys.*, **107**, 026103 (2010).
35. Y. Kimura, H. Shiraki, K. Ishibashi, H. Ishii, K. Itaya, and M. Niwano, *J. Electrochem. Soc.*, **153**, C296 (2006).
36. T. S. Kustandi, W. W. Loh, H. Gao, and H. Y. Low, *ACS Nano*, **4**, 2561 (2010).
37. F. Muller, A. D. Muller, S. Schulze, and M. Hietschold, *J. Mater. Sci.*, **39**, 3199 (2004).
38. A. Yin, M. Tzolov, D. Cardimona, T. Guo, and J. Xu, *IET Circ. Dev. Syst.*, **1**, 205 (2007).
39. S. Park, Y. H. Lee, J. C. Lee, and K. Kim, *Electrochem. Solid-State Lett.*, **9**, D31 (2006).
40. Y. Zhong, C. Xu, L. Kong, and H. Li, *Appl. Surf. Sci.*, **255**, 3388 (2008).
41. N. Tasaltın, S. Öztürk, N. Kılınç, H. Yüzer, and Z. Z. Öztürk, *Appl. Phys. A: Mater. Sci. Process.*, **95**, 781 (2009).
42. S. H. Park, S. Kim, D. J. Lee, S. Yun, Z. G. Khim, and K. B. Kim, *J. Electrochem. Soc.*, **156**, K181 (2009).
43. X. Zhao, U. Lee, S. Seo, and K. H. Lee, *Mater. Sci. Eng.*, **29**, 1156 (2009).
44. K. Kim, M. Kim, and S. Cho, *Korean J. Chem. Eng.*, **22**, 789 (2005).
45. J. Kim, S. Khanal, M. Islam, A. Khatri, and D. Choi, *Electrochem. Commun.*, **10**, 1688 (2008).
46. S. Y. Jeong, M. C. An, Y. S. Cho, D. J. Kim, M. C. Paek, and K. Y. Kang, *Curr. Appl. Phys.*, **9**, S101 (2009).
47. A. Li, F. Müller, A. Birner, K. Nielsch, and U. Gösele, *Adv. Mater.*, **11**, 483 (1999).
48. J. E. Houser and K. R. Hebert, *Phys. Status Solidi A*, **205**, 2396 (2008).
49. S. Z. Chu, K. Wada, S. Inoue, and S. Todoroki, *J. Electrochem. Soc.*, **149**, B321 (2002).
50. See supplementary material at http://dx.doi.org/10.1149/1.3506007 (E-JESOAN-158-018101) for additional information.
51. F. Nasirpouri, P. Southern, M. Ghorbani, A. Irajizad, and W. Schwarzacher, *J. Magn. Magn. Mater.*, **308**, 35 (2007).
52. J. J. Hill, K. Haller, B. Gelfand, and K. J. Ziegler, *ACS Appl. Mater. Interfaces*, **2**, 1992 (2010).
53. S. L. Pan, D. D. Zeng, H. L. Zhang, and H. L. Li, *Appl. Phys. A: Mater. Sci. Process.*, **70**, 637 (2000).

Downloaded 29 Dec 2010 to 159.226.100.225. Redistribution subject to ECS license or copyright; see http://www.ecsdl.org/terms_use.jsp